

Quasi-classical trajectories study of $\text{Ne}_2\text{Br}_2(B)$ vibrational predissociation: Kinetics and product distributions

Wilmer Arbelo-González,¹ Maykel L. González-Martínez,^{1, a)} Stewart K. Reed,² Jesús Rubayo-Soneira,¹ and Dmitrii V. Shalashilin²

¹⁾*Departamento de Física General, Instituto Superior de Tecnologías y Ciencias Aplicadas, Habana 10600, Cuba*

²⁾*School of Chemistry, University of Leeds, Leeds LS2 9JT, United Kingdom*

The vibrational predissociation of the $\text{Ne}_2\text{Br}_2(B)$ van der Waals complex has been investigated using the quasi-classical trajectory method (QCT), in the range of vibrational levels $v' = 16\text{--}23$. Extensive comparison is made with the most recent experimental observations [Pio *et al.*, *J. Chem. Phys.* **133**, 014305 (2010)], molecular dynamics with quantum transitions (MDQT) simulations [Miguel *et al.*, *Faraday Discuss.* **118**, 257 (2001)], and preliminary results from 24-dimensional Cartesian coupled coherent state (CCCS) calculations. A sequential mechanism is found to accurately describe the theoretical dynamical evolution of intermediate and final product populations, and both QCT and CCCS provide very good estimates for the dissociation lifetimes. The capabilities of QCT in the description of the fragmentation kinetics is analyzed in detail by using reduced-dimensionality models of the complexes and concepts from phase-space transport theory. The problem of fast decoupling of the different coherent states in CCCS simulations, resulting from the high dimensionality of phase space, is tackled using a re-expansion scheme. QCT ro-vibrational product state distributions are reported. Due to the weakness of the vdW couplings and the low density of vibrational states, QCT predicts a larger than observed propensity for $\Delta v' = -1$ and -2 channels for the respective dissociation of the first and second Ne atoms.

PACS numbers: 82.37.Np, 34.50.Ez, 82.20.Bc, 31.15.xg

Keywords: vibrational predissociation; van der Waals clusters; quasi-classical trajectories; quantum dynamics

I. INTRODUCTION

Studying the influence of size-selected solvents on the structure and dynamics of molecular systems is essential in understanding both molecular energy transfers and the transition from the gas to condensed phase.

In this regard, clusters of rare gas (Rg) atoms doped with a diatomic halogen (BC) are particularly convenient for at least two reasons: (1) the weakness of the van der Waals (vdW) interactions provides a means to effectively ‘separate’ the diatom from the environment, which in turn allows a relatively simple identification of the different energy transfer mechanisms at the state-to-state level; and (2) the number n of Rg atoms can be spectroscopically selected for their addition induces a known blueshift in the vibronic transition $B(v') \leftarrow X(v=0)^{1-3}$.

These weakly bound complexes have been the subject of intense scrutiny since the pioneering experiments of Levy and co-workers^{1,2,4-6} and the theoretical work of Beswick, Jortner and Delgado-Barrio^{7,8} in the late seventies. In their experiments, Levy and co-workers used laser-induced fluorescence to study Rg_nI_2 molecules based on He, Ne and Ar with up $n = 7$ I atoms.

Following the laser-induced vibrational excitation of BC, the energy is usually redistributed within the molecule leading to the breaking of the vdW bonds. This

process is known as vibrational predissociation (VP) and provides significant information, for instance, on the dynamics of intramolecular vibrational energy redistribution (IVR). Rotational, electronic and other predissociation processes are possible. In the former, rotational de-excitation of the BC molecule directly provides enough energy for fragmentation. In electronic predissociation, non-adiabatic transitions to repulsive electronic states of BC may instead lead to dissociation of the chemically bonded molecule. This was first observed in $\text{Ar}_n\text{I}_2^{5,6}$ and recently studied in HeBr_2 and NeBr_2^9 . In general, the dependence of the transitions on the details of the potential energy surfaces (PESs) as well as on the available energy makes it possible to extract useful information on binding energies and electronic couplings.

The VP of vdW complexes is by far the predominant dissociation process and as such has been the most extensively studied. Depending on the vibrational state excited, vdW systems fragment following one or several elementary steps, which usually include direct dissociation, different IVR regimes, evaporative cooling (EC), etc. For example, the VP of Ne_nBr_2 clusters is described in references 10 and 11. Each step may have different accessible final states and characteristic kinetics which manifest themselves in experiments through distinctively structured product state distributions as in the case of ArCl_2^{12} , HeBr_2 and $\text{NeBr}_2^{13,14}$.

All of the above work (and considerably more) has proved through the years that, despite their apparent simplicity, even small vdW aggregates with $n = 1, 2$ undergo a wide variety of processes that are representative

^{a)}Electronic mail: m.l.gonzalez-martinez@durham.ac.uk; Current address: Department of Chemistry, Durham University, Durham DH1 3LE, United Kingdom

of most of the dynamical pathways observed in more complex, and conventionally bonded, molecules¹⁵. Hence, vdW systems have become valuable prototypes in the analysis of both inter- and intramolecular energy transfers.

For small molecules, exact quantum mechanical calculations (EQM) can be performed with modern computers and algorithms. Being essentially exact, at least to the accuracy of the PESs, these calculations have provided a rigorous picture of the VP process. More recently, they have also addressed in detail the problem of IVR dynamics and the role played by continuum resonances in triatomic systems^{16–22}. Quantum calculations on larger complexes almost inevitably use various approximate methods and there are just a few EQM studies in the literature. In 2001, Meier and Manthe studied the VP of Ne_2I_2 using the multiconfiguration time-dependent Hartree method²³ and although vibrational branching ratios were compared with the experiment², the main aim of their work was to provide a benchmark for future developments in the methodology. In 2005, García-Vela proposed a full-dimensional, fully-coupled wave packet method and used it to study the VP of He_2Cl_2 ²⁴, obtaining good agreement with experimental lifetimes and rotational distributions thus providing a test for the accuracy of the PES employed.

Yet, time-dependent, fully detailed investigations of energy transfers in vdW molecules containing more than one or two Rg atoms still pose a considerable challenge for both experiments and EQM calculations. In the former, researchers should be able to identify and characterize all intermediate complexes, as well as address their dynamical evolution. In the latter they have to cope with the increasing number of degrees of freedom (DOF) and large basis sets that eventually make the computational cost prohibitive. Thus, in the investigation of larger systems hybrid quantum-classical, *e.g.* molecular dynamics with quantum transitions (MDQT) simulations^{10,11,25–27}, and quasi-classical trajectory (QCT) methods have been to date the most widely used practical alternatives.

In fact, most QCT applications have successfully reproduced the fragmentation kinetics for at least several tri- and tetra-atomic complexes. This is the case for molecules such as Ne_nI_2 ($n = 1, 2$)^{19,28,29}, HeICl ³⁰ and NeBr_2 ^{14,31} in which many classical predictions were later confirmed by EQM³². More recently, some of us have explored the extent to which the Gaussian weighted (GW) trajectory method^{33,34} adds to the applicability of QCT in the study of RgBr_2 ($\text{Rg} = \text{He}, \text{Ne}, \text{Ar}$) molecules³⁵. We found that GW may enhance the QCT description of product state distributions both quantitative and qualitatively, especially if only a few vibrational states are populated or calculations are performed very close to a channel closing. However, in cases such as the VP of NeCl_2 ³⁶ and generally, when IVR takes place in the sparse regime and plays a significant role, it seems that only quantum mechanical calculations can be compatible with the experimental observations. Hence, despite the

success of many previous implementations of QCT, the validity of classical concepts in the context of the VP of vdW aggregates is yet to be clarified. At last, complementary studies addressing the dynamical (in)stability of these systems exist in the literature. The analysis of phase-space bottlenecks in the predissociation of HeI_2 was used as a benchmark in the foundation of phase-space transport theory (PSTT)^{37–41}. More recently, irregular variations of decay rates as well as details of the absorption spectra have been studied through the analysis of the phase-space structure and its evolution with increasing excitation energy^{42–45}.

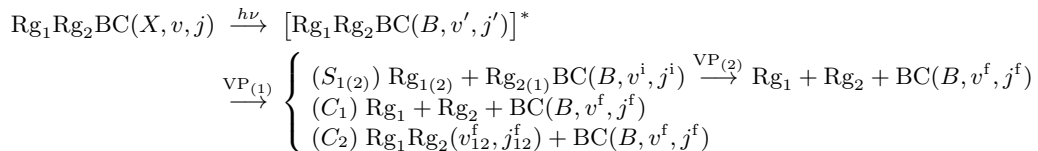
In general, testing the accuracy and reliability of theoretical methods largely depends on detailed experimental data becoming available. In particular, as stated above, realistic kinetic mechanisms can only be obtained if the dynamics of all intermediate species is recorded in the experiment. This has traditionally proved to be quite challenging. For instance, in 1992, Gutmann *et al.*⁴⁶ used picosecond pump-probe spectroscopy to study the VP of Ne_nI_2 with $n = 2–4$ but only registered the formation of I_2 . They therefore inferred the evolution of intermediates by fitting the product dihalogen formation to a sequential first-order kinetic mechanism. In 2010, Pio *et al.*⁴⁷ reported the characterization of the VP of $\text{Ne}_2\text{Br}_2(B)$ at an unprecedented level of detail. Using time- and frequency-resolved pump-probe spectroscopy they were able to record the real time evolution of all complexes involved, propose a kinetic mechanism, and determine time constants and product vibrational state distributions.

In this paper, we report QCT and preliminary Cartesian coupled coherent states (CCCS)^{48,49} calculations on the VP of $\text{Ne}_2\text{Br}_2(B, v' = 16–23)$. We compare both theoretical methods, as well as their ability to reproduce the experimental observations⁴⁷ and previous MDQT predictions¹¹. Our main goal is to build upon the current understanding of the capabilities of QCT in the simulation of VP processes involving larger vdW clusters, and to distinguish whenever possible the results which are intrinsic to the methodology from those that are characteristic to the systems under consideration. Complementary analysis of full-dimensional and simplified models for the VP of the NeBr_2 triatomic complex have been very useful in the interpretation of QCT results and are conveniently discussed.

II. THEORY

A. Vibrational predissociation of a tetra-atomic van der Waals cluster

Assuming that the photo-excitation does not provide enough energy to break the BC bond, the VP of a tetra-atomic vdW aggregate is represented in Scheme 1 where the *i* and *f* superscripts denote intermediate and final states respectively. Two main fragmentation paths are possible, which we refer to as the *sequential* (*S*) and *con-*



SCHEME 1: Representation of the VP of a generic $\text{Rg}_1\text{Rg}_2\text{BC}$ vdW molecule, showing the $(S_{1(2)})$ sequential; as well as concerted (C_1) *without*; and (C_2) *with* molecular formation mechanisms.

TABLE I. Morse parameters for the various pair interactions in Ne_2Br_2 .

	Br ₂ state	D/cm^{-1}	$\alpha/\text{\AA}^{-1}$	$r_{\text{eq}}/\text{\AA}$	Ref.
Br-Br	X	24,557.674	1.588	2.281	16
	B	3,788.0	2.045	2.667	52
Br-Ne	X	45.0	1.67	3.7	20
	B	42.0	1.67	3.9	53
Ne-Ne	X, B	29.36	2.088	3.091	29

certed (C) mechanisms, comprising two channels each. The former is associated with two well-defined dissociation steps and usually dominates as long as direct dissociation prevails over IVR. It leads to the loss of two vibrational quanta and have relatively simple implications in the VP kinetics^{11,29}. The latter becomes increasingly important as IVR dominates, and is very often linked to the loss of more than two vibrational quanta and highly-structured product state distributions. All these features help in distinguishing between the concerted and sequential mechanisms for in the vast majority of cases they lead to the same final products (compare $S_{1(2)}$ and C_1). Finally, when the interaction between the Rg atoms is sufficiently strong and the dynamical evolution allows for favorable configurations, there is a non-negligible probability of formation of a Rg_1Rg_2 molecule.

B. Potential energy surfaces

As seen in Scheme 1 both the ground X and excited B electronic states are, at least in principle, involved in the VP process. Recent studies on the structure of He_2Br_2 and HeICl complexes^{50,51} and EQM calculations on He_2Cl_2 ²⁴ have shown that the global PES for these systems is accurately approximated by

$$V = V_{\text{Rg}_1, \text{BC}} + V_{\text{Rg}_2, \text{BC}} + V_{\text{Rg}_1\text{Rg}_2} + V_{\text{BC}}, \quad (1)$$

where V_{BC} is the interaction potential of the isolated BC molecule, $V_{\text{Rg}_i, \text{BC}}$ ($i = 1, 2$) the vdW PES of the i th triatomic aggregate and $V_{\text{Rg}_1\text{Rg}_2}$ the potential describing the Rg_1 - Rg_2 interaction.

Here, we extrapolate these results and in a first step, we express the global PESs for the Ne_2Br_2 complex in

the form (1). It is important to note that, even if this proves to be a good approximation for $\text{Rg} = \text{He}$ and Ne due to the weakness of the vdW bonds, neglecting 4-body contributions in the global PES of clusters containing heavier Rg atoms could eventually fail. Secondly, by using pairwise additive potentials for the terms $V_{\text{Rg}_i, \text{BC}}$, we neglect 3-body contributions to the triatomic vdW PES. Although this is known to be a good approximation for the B electronic state, which is where the VP process takes place, it is only partially adequate for the ground state^{54,55}. In particular, there is theoretical⁵⁶ and experimental⁵⁷ evidence for an additional minimum at linear configurations in the PES of the X state, which cannot be reproduced by pairwise interactions. The topology of the two electronic states is in fact similar but the linear minimum for the B state moves to a longer distance and becomes much shallower compared to the X state, which makes a pairwise additive description adequate for the former and not the latter. Nevertheless, the calculations presented here refer to the fragmentation induced by the photo-excitation of the T-shaped isomer which can be correctly reproduced in the pairwise additive approximation. All pair interactions are analytically modeled by Morse functions, the parameters for which have been taken from the literature and are summarized in Table I.

C. Quasi-classical trajectories

1. System model

A particular Jacobi association diagram yields the most convenient set of coordinates to describe the unimolecular dissociation of a triatomic RgBC vdW complex. Two Jacobi vectors are involved, \mathbf{r} which conventionally runs from the heaviest to the lightest of atoms B or C, and \mathbf{R} , from the diatom's center of mass towards the Rg atom. Among its main advantages are the symmetrical decomposition of the molecular PES, the explicit use of a dissociation coordinate and an associated diagonal kinetic operator. It is therefore common when studying larger vdW aggregates, *i.e.* $\text{Rg}_1 \dots \text{Rg}_n \text{BC}$, to choose a 'generalized' set of vectors \mathbf{r} , \mathbf{R}_i ($i = \overline{1, n}$) which inherits most of the aforementioned advantages. These are not actually Jacobi co-ordinates but are referred to as satellite or bond co-ordinates. Their main drawback

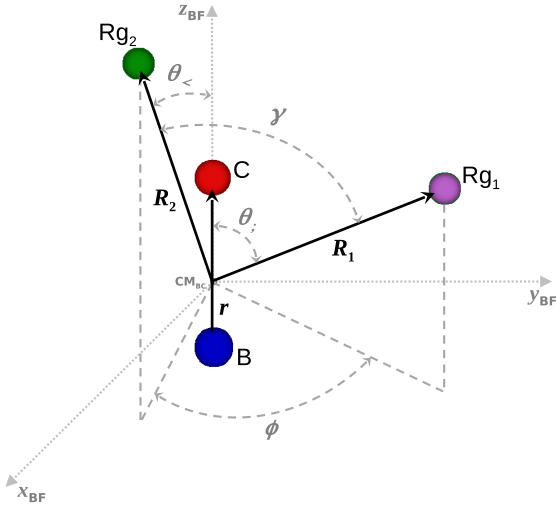


FIG. 1. (Color online) Coordinate set for a prototypical $\text{Rg}_1\text{Rg}_2\text{BC}$ vdW molecule in its body-fixed reference frame.

being a non-diagonal kinetic operator.

The total angular momentum of a tetra-atomic vdW system is given by $\mathbf{J} = \mathbf{l}_1 + \mathbf{l}_2 + \mathbf{j}$, where \mathbf{l}_i is the end-over-end orbital angular momentum of atom Rg_i with respect to BC, and \mathbf{j} the rotational angular momentum of BC. Using satellite coordinates and keeping \mathbf{J} at zero, the set of coordinates reduces to $\{r, R_1, R_2, \theta_1, \theta_2, \phi\}$. These

and

$$\begin{aligned} \mathbf{j}^2 = \mathbf{l}_1^2 + \mathbf{l}_2^2 + 2\mathbf{l}_1 \cdot \mathbf{l}_2 = P_{\theta_1}^2 + P_{\theta_2}^2 + 2P_{\theta_1}P_{\theta_2} \cos \phi - 2 \sin \phi \left(\frac{\cos \theta_2}{\sin \theta_2} P_{\theta_1} + \frac{\cos \theta_1}{\sin \theta_1} P_{\theta_2} \right) P_{\phi} \\ + \left(\frac{1}{\sin^2 \theta_1} + \frac{1}{\sin^2 \theta_2} - 2 \cos \phi \frac{\cos \theta_1 \cos \theta_2}{\sin \theta_1 \sin \theta_2} - 2 \right) P_{\phi}^2. \end{aligned} \quad (6)$$

The non-diagonal coupling term, $\mathbf{P}_1 \cdot \mathbf{P}_2$, can be expressed as

$$\begin{aligned} \mathbf{P}_1 \cdot \mathbf{P}_2 = P_{R_1} P_{R_2} \cos \gamma - \frac{\cos \phi}{R_1 R_2 \sin \theta_1 \sin \theta_2} P_{\phi}^2 \\ + \frac{\cos \theta_1 \cos \theta_2 \cos \phi + \sin \theta_1 \sin \theta_2}{R_1 R_2} P_{\theta_1} P_{\theta_2} + \frac{\sin \theta_1 \cos \theta_2 \cos \phi - \cos \theta_1 \sin \theta_2}{R_2} P_{R_1} P_{\theta_2} \\ + \frac{\cos \theta_1 \sin \theta_2 \cos \phi - \sin \theta_1 \cos \theta_2}{R_1} P_{R_2} P_{\theta_1} - \frac{\sin \theta_1 \sin \phi}{R_2 \sin \theta_2} P_{R_1} P_{\phi} - \frac{\sin \theta_2 \sin \phi}{R_1 \sin \theta_1} P_{R_2} P_{\phi} \\ - \frac{\cos \theta_1 \sin \phi}{R_1 R_2 \sin \theta_2} P_{\theta_1} P_{\phi} - \frac{\cos \theta_2 \sin \phi}{R_1 R_2 \sin \theta_1} P_{\theta_2} P_{\phi}, \end{aligned} \quad (7)$$

with

$$\cos \gamma = \sin \theta_1 \sin \theta_2 \cos \phi + \cos \theta_1 \cos \theta_2. \quad (8)$$

Finally, in the interpretation of our results, models with two and three DOFs (2/3-DOF) are used for the intermediate RgBC complex. The 3-DOF model is a full-dimensional $\mathbf{J} = \mathbf{0}$ approximation of RgBC . The phase-space variables span a subspace of Γ , *i.e.* $\Gamma_3 =$

have been depicted in Fig. 1. Choosing \mathbf{J} to be zero is a well-justified constraint when studying the photodissociation of rotationally cold species⁵⁸ as produced in the experiment through a supersonic free jet expansion⁴⁷. The complete set of variables in classical phase space Γ is finally obtained by adjusting the respective conjugate momenta so that the Hamilton function reads⁵⁹

$$\begin{aligned} \mathcal{H}^{J=0} = \mathcal{H}_{\text{BC}} + \sum_{i=1}^2 \frac{1}{2\mu_{\text{Rg}_i, \text{BC}}} \left(P_{R_i}^2 + \frac{\mathbf{l}_i^2}{R_i^2} \right) + \frac{\mathbf{P}_1 \cdot \mathbf{P}_2}{m_B + m_C} \\ + V_{\text{vdW}}(\mathbf{r}, \mathbf{R}_1, \mathbf{R}_2), \end{aligned} \quad (2)$$

where

$$\mathcal{H}_{\text{BC}} \stackrel{\text{def}}{=} \frac{1}{2\mu_{\text{BC}}} \left(P_r^2 + \frac{\mathbf{j}^2}{r^2} \right) + V_{\text{BC}}(r) \quad (3)$$

and

$$V_{\text{vdW}}(\mathbf{r}, \mathbf{R}_1, \mathbf{R}_2) \stackrel{\text{def}}{=} V(\mathbf{r}, \mathbf{R}_1, \mathbf{R}_2) - V_{\text{BC}}(r). \quad (4)$$

Here, $\mu_{\text{Rg}_i, \text{BC}}^{-1} = m_{\text{Rg}_i}^{-1} + (m_B + m_C)^{-1}$ and $\mu_{\text{BC}}^{-1} = m_B^{-1} + m_C^{-1}$ are the inverse of the appropriate reduced masses, while the angular momenta

$$\mathbf{l}_i^2 = P_{\theta_i}^2 + \frac{P_{\phi}^2}{\sin^2 \theta_i}; \quad i = 1, 2 \quad (5)$$

$\{r, R, \theta, P_r, P_R, P_{\theta}\}$, and all relevant formulae can be easily obtained from Eqs. (2)–(4) or the literature, *e.g.* Ref. 35. The 2-DOF is constructed by additionally fixing $\theta = \pi/2$, corresponding to the equilibrium configuration of NeBr_2 in the B electronic state. The phase state is thus $\Gamma_2 = \{r, R, P_r, P_R\}$ and all necessary formulae can be obtained by simplification of the 3-DOF. In particular, several results can be better understood by

analyzing the structure of classical phase space for the 2-DOF model. To this end, we have used Poincaré surfaces of section (SOS), which are a powerful visual tool when considering systems with two DOF⁶⁰. All SOS employed here were constructed from trajectory intersections with the hypersurface ($r = r_{\text{eq}}, R, P_r \geq 0, P_R$), where r_{eq} is the equilibrium bond length of BC.

2. Initial Conditions

In general, the QCT simulation of photo-induced processes requires the initial conditions to closely match those recreated in the experiment⁵⁸. The latter are however quantum in nature, and are often quite difficult to determine and reproduce classically, especially for polyatomic systems. Obviously, the workarounds commonly used in systems with strong inter-/intramolecular interactions⁶¹ are not applicable here and quantum distributions need to be calculated from the molecular wave function.

Although the rigorous form of the initial wave function is known to depend on the particular shape of the laser pulse, *cf.* Ref. 20, we assume that the pump laser acts during an extremely short time and the system undergoes a perfect vertical transition. The Schrödinger equation for the tetra-atomic system in both the ground and excited states is solved using the variational method proposed in Ref. 62. Then, the X -state wave function is used to calculate the probability distributions (statistical weights) for all relevant variables, while the eigenvalues from the B -state determine the VP energetics, as in our previous work^{31,35}. Once the X - and B -state quantum problems are solved, QCT initial conditions are calculated following the algorithm proposed in Ref. 63 (with only a few minor modifications):

1. a set of ‘quantum’ numbers $\{l_1, l_2, j\}$ is selected using their respective distributions—checking it satisfies the triangle condition $\Delta(l_1, l_2, j)$ to ensure compatibility with $\mathbf{J} = \mathbf{0}$;
2. the angles $\theta_1, \theta_2, \gamma$ are generated following the appropriate distributions, and ϕ calculated from Eq. (8);
3. the system of non-linear equations (5) and (6) is solved for the angular momenta $P_{\theta_1}, P_{\theta_2}$ and P_ϕ ;
4. r is generated from the calculated distribution, and the value of j used to calculate P_r from Eq. (3). Here, \mathcal{H}_{BC} is conveniently replaced with $\mathcal{E}_{\text{BC}}^{B,v'}$, *i.e.* the eigenvalue corresponding to the $(B, v', j' = 0)$ state of BC⁶², and the sign of P_r randomly chosen;
5. R_1 and R_2 are generated with the corresponding distribution, and approximate conjugate momenta

calculated using

$$P_{R_i}^{\text{app}} = \pm \sqrt{2\mu_{\text{Rg}_i, \text{BC}} \left(\mathcal{E}_{\text{Rg}_i, \text{BC}}^{B,v'} - \frac{l_i^2}{2\mu_{\text{Rg}_i, \text{BC}} R_i^2} - V_{\text{Rg}_i, \text{BC}} \right)}, \quad (9)$$

where $\mathcal{E}_{\text{Rg}_i, \text{BC}}^{B,v'}$ is the eigenvalue corresponding to the Rg_iBC triatomic aggregate with BC in its (B, v') state⁶², and the sign of the momentum is once again randomly chosen;

6. finally, the energy associated to the non-diagonal kinetic term $\mathbf{P}_1 \cdot \mathbf{P}_2$ and $V_{\text{Rg}_1 \text{Rg}_2}$ is redistributed within the vdW modes by writing $P_{R_{1(2)}} = P_{R_{1(2)}}^{\text{app}} + \Delta_{1(2)}$, where Δ_1 and Δ_2 are quantities to be determined. Their calculation requires evaluating $\mathcal{H}^{J=0} = \mathcal{E}^{B,v'}$, the energy of the tetra-atomic complex with Br_2 in the (B, v') state, using the set of values $\{r, R_1, R_2, \theta_1, \theta_2, \phi, P_r, P_{R_1}^{\text{app}}, P_{R_2}^{\text{app}}, P_{\theta_1}, P_{\theta_2}, P_\phi\}$, as well as the additional constrain $P_{R_1}^{\text{app}}/P_{R_2}^{\text{app}} = \Delta_1/\Delta_2$.

Steps 1–6 are repeated until N_{tot} initial conditions are obtained.

3. From classical magnitudes to observables

We have recently discussed the statistical handling of QCT results for comparison with experimental observables in the specific case of the VP of triatomic vdW systems³⁵. There is however one fundamental difference between the process in tri- and tetra-atomic molecules, namely, the possible formation in the latter of an intermediate complex. For consistency, the general methodology is only summarized here with emphasis on the changes made in order to analyze the QCT results in our specific case.

When the molecule completely dissociates, $V_{\text{vdW}} \rightarrow 0$ and both \mathbf{j} and \mathcal{H}_{BC} become integrals of motion with the latter corresponding to the classical energy of the BC fragment, E_{BC} . The final semi-classical ro-vibrational quantum numbers for the i th dissociated trajectory, *i.e.* $v_{c,i}^f$ and $j_{c,i}^f$, are then rigorously constant and are given by

$$\begin{aligned} v_{c,i}^f &= \frac{1}{2\pi\hbar} \oint P_r dr - \frac{1}{2} \\ &= \frac{\sqrt{2\mu_{\text{BC}}}}{\pi\hbar} \int_{r_{\text{min}}}^{r_{\text{max}}} \sqrt{E_{\text{BC},i} - V_{\text{eff}}} dr - \frac{1}{2}, \quad (10) \end{aligned}$$

where V_{eff} is the effective interaction potential of BC (including the centrifugal term) and the closed integral is evaluated over one BC vibrational period⁶⁴ (r_{min} and r_{max} are the classical turning points), while

$$j_{c,i}^f = \frac{1}{2} \left[\sqrt{1 + 4 \left(\frac{j_i}{\hbar} \right)^2} - 1 \right], \quad (11)$$

which results from $j_i^2 = j_{c,i}^f(j_{c,i}^f + 1)\hbar^{265}$. Due to the weakness of the vdW interaction, the BC vibrational state in the intermediate complex, $v_{c,i}^i$, can be estimated using Eq. (10). This requires replacing the final state magnitudes with approximate values for the intermediate state, despite these not being rigorously defined.

In what follows, we neglect the quantized nature of the rotational DOF as it has a very high density of states and refer simply to channel $\Delta v' = v^f - v'$ by the associated final vibrational quantum number, v^f .

In the procedure known as *histrogram* or *standard binning* (SB), the probability density $P(M, v^f)$ that a given observable has the value M and the final BC vibrational state is v^f can be formally written as

$$P_{\text{SB}}(M, v^f) = \int d\mathbf{\Gamma} \rho(\mathbf{\Gamma}) \delta[M(\mathbf{\Gamma}) - M] \Xi[v^f(\mathbf{\Gamma}); v^f, 1], \quad (12)$$

where $\rho(\mathbf{\Gamma})$ is the probability distribution of the initial phase space state, $\mathbf{\Gamma}$, and

$$\Xi(x; x^*, \Delta) = \frac{1}{\Delta} \Theta(x^* + \Delta/2 - x) \Theta(x - x^* + \Delta/2). \quad (13)$$

$\delta(x)$ and $\Theta(x)$ are respectively the Dirac and Heaviside functions. $M(\mathbf{\Gamma})$ and $v^f(\mathbf{\Gamma})$ are the final values of the observable and the vibrational action in terms of $\mathbf{\Gamma}$. It is relatively easy to see from Eq. (13) that Ξ defines a square barrier function of x , which equals $1/\Delta$ on $[x^* - \Delta/2, x^* + \Delta/2]$ and 0 everywhere else. Also, P_{SB} in Eq. (12) is normalized to 1.

In practice, P_{SB} is estimated by means of the Monte-Carlo expression

$$P_{\text{SB}}(M_k, v^f) \approx \frac{1}{N_{\text{diss}}} \sum_{i=1}^{N_{\text{diss}}} \Xi[M(\mathbf{\Gamma}_i); M_k, \alpha_k] \times \Xi[v^f(\mathbf{\Gamma}_i); v^f, 1], \quad (14)$$

where M_k is the k th midpoint in the $\{M\}_{k=1}^K$ set partition of the interval $[M_{\text{min}}, M_{\text{max}}]$, $\alpha_k = M_{k+1} - M_k$ and N_{diss} is the total number of dissociated trajectories, which is assumed to be large.

In the GW procedure one simply replaces the square barrier function $\Xi[v^f(\mathbf{\Gamma}); v^f, 1]$ in Eq. (14) with the Gaussian

$$g[v^f(\mathbf{\Gamma}); v^f, \epsilon] = \frac{\exp\left\{-[v^f(\mathbf{\Gamma}) - v^f]^2/\epsilon^2\right\}}{\pi^{1/2}\epsilon}, \quad (15)$$

in which ϵ is usually kept at 0.05. Hence, P_{GW} is simply

$$P_{\text{GW}}(M_k, v^f) \approx \frac{1}{N_{\text{diss}}} \sum_{i=1}^{N_{\text{diss}}} \Xi[M(\mathbf{\Gamma}_i); M_k, \alpha_k] \times g[v^f(\mathbf{\Gamma}_i); v^f, \epsilon]. \quad (16)$$

In the tetra-atomic case, variations of these general expressions can describe either the intermediate or final

states. To do this, it is sufficient to use the appropriate weight function for the desired state for the second Ξ function in Eq. (14) and the Gaussian function in Eq. (15) respectively. We must note that the weight for the intermediate state is calculated as the product of the weights corresponding to the semi-classical vibrational level of BC and that of the intermediate vdW complex: $w^i = w_1^i(v_c^i) w_2^i(n_c^i)$, where w refers to either Ξ or g . This could dramatically increase the number of trajectories necessary for convergence. Moreover, although Eq. (10) provides a simple means to estimate the semi-classical analogue for the vibrational state of BC, that of the vdW complex is much more difficult to evaluate. A simpler approach, known as the 1GB procedure, uses the total ro-vibrational energy rather than that of the individual states to calculate the corresponding weight: $w^i = w^i(E_{\text{Rg},\text{BC}}^{B,v_c^i})$. Both the $\mathcal{E}_{\text{BC}}^{B,v'}$ and $\mathcal{E}_{\text{Rg},\text{BC}}^{B,v'}$ eigenvalues are involved in this calculation, see Sec. II C 2. The method was proposed by Czako and Bowman⁶⁶ on the basis of rather intuitive arguments and was later theoretically validated by Bonnet and Espinosa-García⁶⁷. In the particular case when the first and second dissociation steps are statistically independent, the total weight can be calculated as the product $w = w^i w^f$. In addition, mixed strategies may be tested by simply using $w = w^{i(f)}$, hence calculating the desired state distributions independently of the final/intermediate vibrational state.

The time evolution of the populations of the various complexes can be obtained by small modifications to the formulae determining survival probabilities, *i.e.* the probability that a given complex has not dissociated at time t , which read³⁵

$$P_{\text{SB}}(t) = 1 - \frac{1}{N_{\text{diss}}} \sum_{i=1}^{N_{\text{diss}}} \Theta(t - t_i),$$

$$P_{\text{GW}}(t) = 1 - \frac{1}{\sum_{i=1}^{N_{\text{diss}}} g_i} \sum_{i=1}^{N_{\text{diss}}} g_i \Theta(t - t_i), \quad (17)$$

with $g_i = \sum_{v,v'} g(v(\mathbf{\Gamma}_i); v, \epsilon)$ and t_i the dissociation time for the i th trajectory. In the particular case of a Rg₂BC cluster, for which t_1 and t_2 are the dissociation times for the first and second Rg atoms, the different populations are explicitly obtained as: (1) $P_4(t) = P(t_1)$, the decay of the parent molecule; (2) $P_3(t) = P(t_2) - P(t_1)$, time evolution of the intermediate RgBC population; and (3) $P_2(t) = 1 - P(t_2)$, formation of the BC fragment. Moreover, (4) $P_3'(t) = P(t_2 - t_1)$ directly represents the decay of the RgBC complex. The reasons for the subscripts will become apparent in Section III A.

4. Simulation details

Batches of $N_{\text{tot}} = 5 \times 10^5$ trajectories were propagated using an adaptive-stepsize Bulirsch-Stoer method⁶⁸. Each trajectory was followed until one of two conditions was fulfilled: (1) the two Ne atoms dissociated,

i.e. $R_{1(2)} \geq R_{\text{diss}}^{\text{QCT}} = 14 \text{ \AA}$; or (2) the propagation time $t = T_{\text{max}} = 1200 \text{ ps}$. Dissociation is said to occur when $R_{1(2)} = 14$, the distance at which the vdW interactions become negligible. The integration parameters were adjusted so that the maximum error in total energy did not exceed $\Delta E = 10^{-5} \text{ cm}^{-1}$, *i.e.* less than $10^{-8} E$. With this choice of parameters all trajectories dissociated at least one Ne atom while over 88–99%, depending on v' , completely fragmented. A typical trajectory requires less than 1 second of CPU time on an Intel® Core™ i7 Q720 (6M Cache, 1.60 GHz) processor.

D. Cartesian coupled coherent states

The CCCS method is a trajectory-based quantum dynamics technique designed to be similar to classical trajectory simulations. The main focus of this paper is the QCT predictions and thus CCCS results are mainly presented to corroborate the conclusions and the quality of the QCT results. Consequently, we will only give a brief outline of CCCS in order to aid comprehension of the results that are included. The interested reader is referred to Ref. 49 which not only describes in detail our previous work on the VP of NeBr₂ but also outlines the extension to larger clusters. A more detailed CCCS study of Ne₂Br₂ will be published in due course⁶⁹.

The QCT method described hitherto is concerned with the point-like nuclei that make up the Ne₂Br₂ cluster whereas the CCCS method allows us to study the time evolution of the associated quantum mechanical wave function. The CCCS method expands the wave function using a basis of coherent states (CS). In CCCS, the CS are Gaussian-shaped wave packets that describe both the position and momentum for each Cartesian DOF of each atom. Thus for Ne₂Br₂, each CS has 24 dimensions. The CS move on the same PES, and according to the same equations as the nuclei in QCT. However, the potential energy for the CS is the convolution of the CS and the PES. In contrast, within the QCT method, the potential energy of a given configuration is simply the value of the PES at that point in configuration space. In CCCS, the convolution may be done in advance of the simulations and it gives the so-called *averaged* or *re-ordered* PES (or equivalently, Hamiltonian) upon which the centers of the CS move.

The amplitudes evolve with time according to an expression derived from Schrödinger’s equation and which depends upon the fact that the basis functions overlap. This overlap couples the amplitudes of the basis functions together. If the basis functions are separated by a sufficiently large distance in the 24-dimensional phase space, they cease to overlap and become decoupled. Once all the basis functions have decoupled, the CCCS method is essentially a semi-classical method. However, even in its semi-classical limit, the CCCS technique takes into account the majority of zero point energy effects.

1. Simulation details

The initial coordinates for the basis functions are determined from a set of bond lengths and momenta so that the total linear and angular momenta of the cluster are zero. For Br–Br, these were chosen from the phase-space trajectory at the energy expectation value of the isolated molecule. In the case of Br–Ne and Ne–Ne, they were chosen randomly from the ground state wave functions of the bonds. Initially, each basis consisted of 400 basis functions and the results have been averaged over 10 different basis sets per Br₂ vibrational level.

As CCCS simulations are considerably more expensive than QCT calculations, a Ne atom is said to have dissociated once the mean distance between it and the Br₂ molecule exceeds $R_{\text{diss}}^{\text{CCCS}} = 10 \text{ \AA}$. Similarly, the second stage dissociation is said to occur when the distance between Br₂ and the remaining Ne exceeds the same cutoff.

In our previous work⁴⁹, we found that the basis functions in the simulations of the VP of NeBr₂ remained coupled until the clusters completely dissociate. In the current work, however, the basis functions decouple much more quickly due to the increased dimension of phase space. Obviously, the time at which each basis function decouples varies greatly but it is typically less than 10 ps: the mean time in one simulation was about 6 ps. As will be discussed later, this leaves comparatively few independent basis functions to describe the dissociating wave function and leads to increased lifetimes.

The calculated lifetimes can be improved by spawning a secondary simulation each time a basis function permanently decouples in which the decoupled basis function is expanded on a new basis of 50 CS. The calculation of the lifetimes is thus a two-part process: first we perform a simulation of the whole wave function expanded on the basis of 400 CS; and then we perform 400 secondary simulations each with 50 basis functions describing one of the basis functions of the original simulation starting from when that basis function decoupled. We found that decoupling invariably occurs before dissociation which makes the combination of the dissociation curves from 400 secondary simulations easier.

The time required to perform the CCCS calculations depends upon the length of time for which the basis functions remain coupled and increases nonlinearly with the number of basis functions. As an example, the mean time for $v = 17$ for 100 ps (10^5 steps), using 400 basis functions was 3.2 days. The mean time for the re-expansions however was 1.3 hours per simulation on Intel® Xeon® ‘Woodcrest’ processors.

III. RESULTS AND DISCUSSION

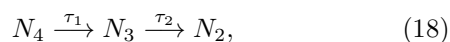
A. Kinetics, lifetimes

1. QCT

PSTT establishes that certain structures in classical phase space (resonant islands, tori, cantori...) act as inter- and intramolecular bottlenecks to the diffusion of trajectories from regions defining ‘reactants’ and ‘products’^{37–39}. A rigorous (classical) kinetic mechanism must therefore reflect the details of these partial obstacles. In addition, a complete rationalization of the energy-dependence of decay rates requires the stability of periodic orbits and the evolution of bifurcations in the phase-space portrait to be addressed in depth. While this is possible and has already been carried out for simple 2-DOF models of molecular systems, including vdW complexes^{42,43,70–72}, its extension to more DOF introduces serious technical difficulties³⁹ and constitutes in itself an active field of research. In fact, further below we use some of these results and a 2-DOF model of NeBr₂ to better understand the relation between product states and dissociation lifetimes, as well as certain features in the time-evolution of the intermediate complex.

Analyzing the phase-space structure of Ne₂Br₂, or even NeBr₂, is however far from our objective here and, at this point, we take advantage of one important experimental conclusion: At least for low v' levels, a simple sequential kinetic mechanism (Section II A) provides an excellent fit to the delay scans (Figs. 7 and 8 in Ref. 47). This is consistent with several results from our QCT calculations: (1) once the Ne₂Br₂ complex decayed into NeBr₂, the only process observed was the fragmentation of the resulting triatomic into Ne and Br₂ products; (2) less than about 0.05% of all trajectories dissociated via the concerted mechanism (subset of all trajectories for which both Ne atoms dissociated within one Br₂ vibrational period, excluding those predicted by the sequential mechanism to dissociate within that time interval⁷³); and (3) no significant statistical correlation was found between the variables defining the intermediate complex and $t_2 - t_1$. The latter confirms, at least from the kinetics viewpoint, that the second dissociation step is nearly statistically independent on the first⁷⁴. All of these observations agree with the fact that: (4) EQM calculations on the VP of NeBr₂ show that direct predissociation dominates within the vibrational range explored here²⁰.

The proposed kinetic mechanism is schematically



where N_4 , N_3 and N_2 stand for the Ne₂Br₂, NeBr₂ and Br₂ populations respectively, while τ_1 and τ_2 are the corresponding lifetimes. Mathematically, Eq. (18) can be

written as

$$\begin{aligned} dN_4/dt &= -k_1 N_4, \\ dN_3/dt &= k_1 N_4 - k_2 N_3, \\ dN_2/dt &= k_2 N_3, \end{aligned} \quad (19)$$

with $k_i = \tau_i^{-1}$, and its solution

$$\begin{aligned} N_4(t) &= N_4(0) \exp(-k_1 t), \\ N_3(t) &= \left[N_3(0) - \frac{k_1 N_4(0)}{k_2 - k_1} \right] \exp(-k_2 t) + \frac{k_1 N_4(0)}{k_2 - k_1}, \\ N_2(t) &= N_{\text{tot}} - N_4(t) - N_3(t), \end{aligned} \quad (20)$$

where $N_4(0) = N_{\text{tot}}$ and $N_3(0) = N_2(0) = 0$. Given the dependence on τ_1 and τ_2 of Eqs. (20), various schemes to extract the lifetimes from survival probability curves become possible. One can: (1, 2) first obtain τ_1 from fits to Ne₂Br₂ decay curves and use this value to get τ_2 from the time dependence of NeBr₂, or alternatively, Br₂ populations; or (3, 4) directly infer both values from the evolution of NeBr₂ or Br₂ populations. Alternatively, taking into account that the individual dissociation times t_1 and t_2 are nearly uncorrelated, one may: (5) directly extract the value of τ_2 by fitting the probability of complete dissociation after a time $t_{21} = t_2 - t_1$ (fragmentation of the triatomic once it is formed) to a single exponential decay. This is implicit in our kinetic mechanism and readily seen by adding the first two equations in (19). Schemes (1)–(4) are somewhat similar to the experimental freedom of determining the lifetimes by measuring the time dependence of the Ne₂Br₂/NeBr₂ signal in a given Br₂ vibrational state, referred to as ‘disappearance’ of the parent complex, and that of the NeBr₂/Br₂ signal in the vibrational states resulting from dissociation, the ‘appearance’ of the daughter molecule, etc. Depending on the signal monitored, different values are obtained in the experiments (and EQM), which provide a measure of IVR^{20,47,75}. However, QCT will yield the same lifetimes no matter what scheme is used (though numerical fitting and convergence will in practice result in small differences). This is easily understood for according to our criteria, the disappearance of Ne₂Br₂ exactly matches the appearance of NeBr₂, etc. As an example, the relevant probability curves, *i.e.* $P_i(t) = N_i(t)/N_{\text{tot}}$, $i = 4-2$ and $P'_3(t)$, corresponding to $v' = 21$ are shown in panel (a) of Fig. 2, together with the respective fits. We have verified that the various schemes yield similar results, and experimental and theoretical lifetimes are summarized in Table II. In the latter, column ‘ v' ’ corresponds to the vibrational level in the B electronic state to which the Ne₂Br₂ molecule is excited by the laser pulse. Column ‘Species(v)’ then corresponds to the molecular product (in the specific vibrational state v) that is monitored in the experiment. ‘ τ_1 ’ and ‘ τ_2 ’ are the lifetimes of Ne₂Br₂ and NeBr₂. In particular, as seen in Eqs. (20), the fragmentation of Ne₂Br₂ depends only on k_1 , which is why no τ_2 is reported in the experiment for this molecule. As discussed above, the theoretical methods yield nearly identical results independently on the probability curve

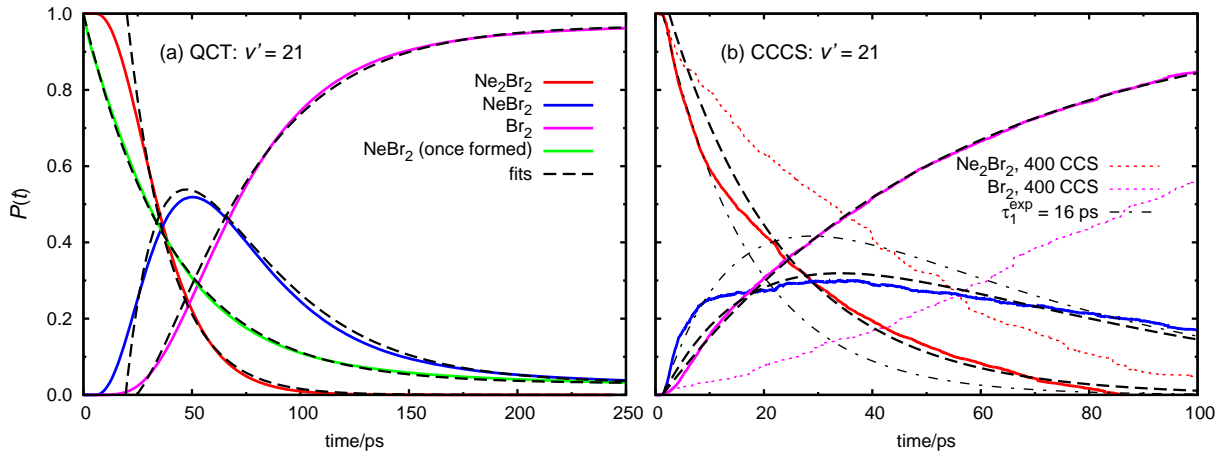


FIG. 2. (Color online) Time evolution of the population of all complexes involved in the vibrational predissociation of $\text{Ne}_2\text{Br}_2(B, v' = 21)$: (a) QCT; and (b) CCCS calculations.

used for the fitting, and a single pair of values τ_1, τ_2 is thus reported for the system (note that no τ_2 value was reported in Ref. 11).

Simple inspection of panel (a) in Fig. 2 shows that the agreement between our fits and QCT calculations is very good, which confirms the accuracy of the kinetic mechanism proposed. This is the general trend for all vibrational levels explored here. Even so, in most cases, small discrepancies occur at short and large times. From

TABLE II. Experimental⁴⁷ and theoretical—this work and MDQT¹¹—lifetimes (in ps) in the vibrational predissociation of $\text{Ne}_2\text{Br}_2(B, v' = 16-23)$.

v'	Species(v)	Experiment		QCT		CCCS		MDQT
		τ_1	τ_2	τ_1	τ_2	τ_1	τ_2	τ_1
16	$\text{Ne}_2\text{Br}_2(16)$			62.1	134.0			
17	$\text{Ne}_2\text{Br}_2(17)$	32±3		48.5	115.9	44.0	98.9	29
	$\text{NeBr}_2(16)$	30±3	88±3					
	$\text{Br}_2(15)$	31±2	82±3					
18	$\text{Ne}_2\text{Br}_2(18)$	28±3		33.8	89.6			
	$\text{NeBr}_2(17)$	27±5	58±5					
	$\text{Br}_2(16)$	28±3	55±4					
19	$\text{Ne}_2\text{Br}_2(19)$			28.0	66.5			24
20	$\text{Ne}_2\text{Br}_2(20)$			23.9	51.1			19
21	$\text{Ne}_2\text{Br}_2(21)$	16±3		19.3	40.5	21.7	53.1	16
	$\text{NeBr}_2(20)$	14±5	30±2					
	$\text{NeBr}_2(19)$	17±4	54±3					
	$\text{Br}_2(19)$	16±2	29±2					
	$\text{Br}_2(18)$	16±2	47±2					
22	$\text{Ne}_2\text{Br}_2(22)$			16.2	34.5			13
23	$\text{Ne}_2\text{Br}_2(23)$			14.1	28.9	15.3	39.4	

the comparison of the classical survival probability curves corresponding to the decay of the Ne_2Br_2 , red curve, and the fragmentation of the intermediate NeBr_2 , green curve, the nature of the plateau usually observed at short times becomes rather clear. It is simply an artifact resulting from both the classical description of the process and the way initial conditions are sampled. More explicitly: there is a minimum time for the gradual classical energy transfer from the Br_2 vibrational mode to dissociate one Ne atom which, in the case of the first decay, has been located close to the vdW minima at the belt-like configuration. In contrast, a quantum vibrational transition may immediately release enough energy for dissociation to occur, as readily seen in CCCS curves from panel (b). The fact that no such feature is observed in the second QCT step further confirms this reasoning for once the first atom is lost, the dynamics would sample more evenly the available phase space and have placed the second Ne atom arbitrarily close to R_{diss} . One may say that this apparent non-exponential behavior (in the fragmentation kinetics) mainly arises from initial state selection⁷⁶.

The reasons for the discrepancies at larger times are more complex and better understood using a 2-DOF model for the VP of NeBr_2 (with $\theta = \pi/2$). Analysis of the SOS shows a 1:10 nonlinear resonance (for $v' = 21$) surrounding the stable central region around the point ($R = R_{\text{eq}}, P_R = 0$). This resonance occupy a significant proportion of the available phase space. The extent to which such intramolecular bottlenecks affect the overall time evolution of the classical ensemble depends on the proportion of initial conditions lying inside or relatively close to their boundaries. Actually, early work on PSTT showed that kinetic mechanisms can be conveniently modified to account for such behavior³⁷. In our case, only a relatively low percent of trajectories, about 0.3% for $v' = 21$ in Fig. 2, show a strong non-

exponential behavior, *always* after the dissociation of the first Ne atom. This is most likely due to remaining lower-dimensionality tori, which have been recently demonstrated to play a significant role as bottlenecks between diffusive and statistical behavior in systems with more than two DOF⁷⁷.

Given all of the above, the actual equations used to produce the fits shown in Fig. 2 are in fact slightly modified versions of Eqs. (20) which account for both sources of non-exponential behavior. That at low times is ‘avoided’ by fitting from $t_0^{v'} > 0$, while the long-time behavior is modeled by adding a given constant (which equals the asymptotic proportion of non-dissociated trajectories at each v'). We should note that, after adding this constant, all coefficients need to be adequately modified to recover the correct behavior at $t = 0$.

2. CCCS

The survival probabilities for the different complexes for $v' = 21$, as calculated using CCCS, are shown in panel (b) of Fig. 2. In contrast to panel (a): (1) dotted lines (labeled ‘400 CCS’) correspond to the initial CCS simulations with 400 basis functions, the re-expansion of which gives the main curves; (2) the survival probability of NeBr₂ once it is formed from the Ne₂Br₂ cluster is not presented, as this time is ill-defined in the CCCS calculations; and (3) dot-dashed lines (labeled ‘ $\tau_1^{\text{exp}} = 16$ ps’) uses the experimental value⁴⁷ to model the time evolution at short times. The fits are obtained using the same sequential kinetic mechanism as for QCT, and the lifetimes given in Table II are from fitting the modified versions of Eqs. (20) to the CCCS data, also necessary here, mainly to account for those basis functions that do not dissociate.

Theoretically, CCCS will provide a quantum mechanical description as long as the basis functions remain coupled, which ideally should be for a time comparable to the process of interest. As in our previous study of the NeBr₂ system⁴⁹, CCCS removes the nonphysical plateau shown by QCT at short times, thus accurately reproducing the initial quantum dynamics. However, it becomes harder to fit the results of CCCS to a simple model of sequential dissociation at longer times. This could be because quantum mechanics makes non-sequential dissociation more likely. Previously, non-sequential IVR-EC contributions to dissociation were found to be important in MDQT simulations for $v > 14$ where they account for one fifth of all dissociative trajectories¹¹. Also, experiments⁴⁷ seem to indicate that complicated non-sequential mechanisms are important for $v > 19$. However, it would be premature to claim that the current CCCS simulations prove the pertinence of non-sequential mechanisms. Although our re-expansion technique (Section IID 1) greatly increases the time scale at which CCCS works, it is still below the range of hundreds of picoseconds required for the description of the whole fragmentation process. At such long

time scales, CCCS works as a semi-classical technique running largely uncoupled CS on the averaged potential. It accounts for zero point energy effects but not for the full quantum coupling in phase space. We are currently working on strategies to further extend the coupling time between the CS in the quantum simulations. More detailed (and costly) investigations are necessary and the results will be published elsewhere⁶⁹.

In general, both QCT and CCCS predictions are in very good agreement with each other, thus CCCS confirming the good quality of much simpler and less expensive QCT results. Both methods are also in good agreement with the experimental lifetimes, over the whole range of initial vibrational states. However, although providing a near-quantitative description of the kinetics, they seem to consistently yield larger than observed values. In the case of QCT, this may be intrinsic to the methodology and the existence of low-dimensional tori in classical phase space. Additional CCCS calculations are needed in order to verify whether this is inherent to the method or due to, *e.g.* an inadequate representation of the PES or the wave function.

B. PSTT, SB, GW and QCT dissociation times

Based on PSTT, it seems reasonable to expect that trajectories with the highest Gaussian weights, which contribute the most to the GW curves and correspond to vibrational actions the closest to integer values, do not necessarily explore the same regions in phase space than the whole ensemble and could therefore undergo different kinetics. Hence, at least in principle, applying the SB or GW methods can produce different time evolution probability curves (Section IIC 3) and correspondingly, result in different lifetimes. In turn, GW results should be the closest to the experimental values for this method effectively eliminates trajectories which finish in nonphysical vibrational channels. Quite surprisingly, no significant differences between SB and GW lifetimes were found in our previous calculations on the VP of RgBr₂ (Rg = He, Ne, Ar) molecules (see Fig. 1 in Ref. 35), where several possible reasons were proposed.

In the VP of Ne₂Br₂ studied here, the predictive capabilities of GW can be additionally tested for the experiment provides detailed information on the kinetics associated to different vibrational channels for $v' = 21$ (see Table II). Unfortunately, once again, our calculations seem to corroborate that both the SB and GW methods result in nearly identical lifetimes, with no significant variation between the various vibrational channels. In other words: the GW procedure was found to be unable to provide vibrational resolution in the dissociation lifetimes. In the rest of this section, we will show that 2- and 3-DOF models for the VP of NeBr₂ are very helpful in the detailed analysis of this issue.

The relation between trajectory lifetimes and final states is rather intricate, as is apparent from Fig. 3. Panel

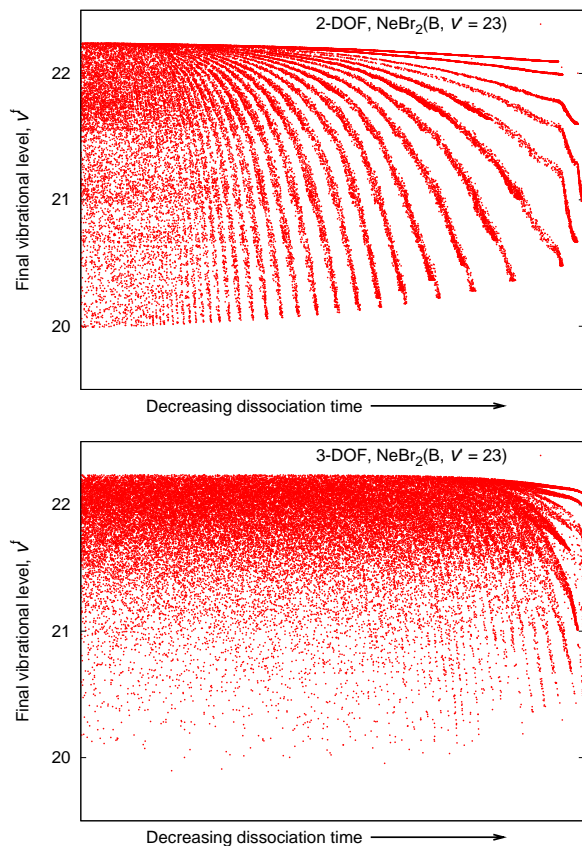


FIG. 3. (Color online) Dependence between dissociation lifetimes and final vibrational states in the vibrational predissociation of NeBr_2 from $v' = 23$: (a) 2-DOF; (b) 3-DOF model.

(a) shows how final vibrational states relate to the individual dissociation times for an ensemble of 5×10^4 trajectories in the 2-DOF model. As readily seen, there is a relative insensitivity between these magnitudes for trajectories with longer to medium lifetimes, while a specific pattern arises for shorter dissociation times. These finger-like structures can be understood by analyzing the VP process in phase space, in the spirit of PSTT. For simplicity we will only introduce here the essential elements of the methodology that are required by our interpretation. Further information can be found in the seminal work of Davis *et al.*, most notably in Ref. 37.

Figure 4 depicts the main structures in the SOS of a 2-DOF model for a generic triatomic. The SOS is constructed by the procedure described in Section IIC and the molecule is assumed to dissociate if $R \geq R_{\text{diss}}$. The *separatrix* (continuous red line) encloses the interaction region and constitutes the intramolecular bottleneck to dissociation. The fingers (green/blue dashed lines) limit the region available to the outgoing/incoming flux. All dissociating trajectories will intersect the region enclosed by the outgoing fingers (dashed, green) and the separatrix, once only. Thus, after leaving the interaction region,

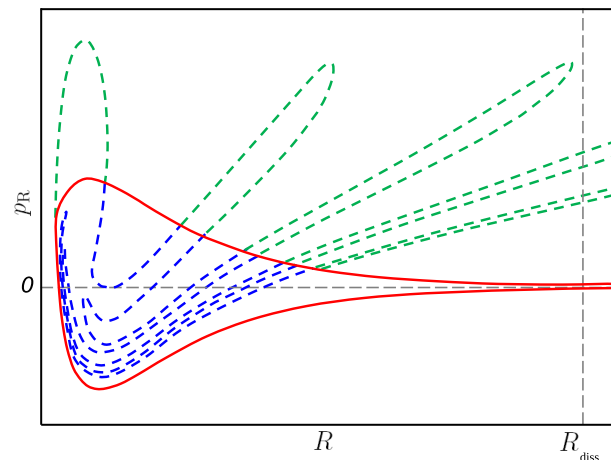


FIG. 4. (Color online) Schematic view of the main structures in the SOS of a 2-DOF model for the VP of a generic triatomic: separatrix (red, continuous line), outgoing (green, dashed line) and incoming (blue, dashed line) fluxes.

any given trajectory will inevitably dissociate and consecutive intersections will lie in different fingers as $R(t)$ increases monotonically. All that rests now is to notice that trajectories closer to the fingers' 'tips', *i.e.* those with the largest P_R , correspond to the smallest v available (and vice versa). The previous follows from the fact that the total energy E is fixed in the ensemble. At last, the existence of finger-like structures like those in Fig. 3 will strongly depend on the characteristics of the dynamics within the interaction region. If completely stochastic, initial conditions will be effectively 'forgotten' and trajectories will access the outgoing fingers after exploring the interaction region during a random propagation time. No correlation between dissociation times and final vibrational states will be observed. On the other hand, if intermolecular couplings are not strong enough, a subset of trajectories whose initial conditions lie within a specific region inside the separatrix will directly access the outgoing fingers. These trajectories will therefore dissociate rapidly and a pattern will arise. Following this line of reasoning, it is not difficult to see why the structures in panel (a) of Fig. 3 have precisely their shape. Panel (b) in the same figure shows results for the 3-DOF model of NeBr_2 . The similarities between the 2- and 3-DOF models are evident, although the finger-like structures get increasingly blurred the larger the number of DOF. The number of such finger-like structures depends on the kinetic energy available to dissociation, hence decreasing with increasing vibrational excitation. Additional calculations show that all structures completely disappear for energies above the linearization threshold (Br-Ne-Br configuration barrier).

TABLE III. Energies (in cm^{-1}) in the vibrational predissociation of $\text{Ne}_2\text{Br}_2(B, v')$ (see text for full details).

v'	$\Delta\mathcal{E}_{\text{Br}_2}^{B, v'-1}$	$D_0^{\text{NeBr}_2(B, v')}$	$D_0^{B, v'}$	$E_{\text{avail}}^{v'-1}$	$E_{\text{avail}}^{v'-2}$
16	107.4	63.3	137	33	81
17	103.8	63.1	137	29	74
18	100.2	62.8	137	26	67
19	96.6	62.6	137	22	60
20	93.1	62.3	136	19	54
21	89.5	62.0	136	15	47
22	85.9	62.5	135	13	40
23	82.3	62.4	135	9	33

C. Product state distributions

Ro-vibrational product state distributions were calculated from the ensemble of quasi-classical trajectories as described in Section II C 3. As many relevant features of these observables strongly depend on the energetics of the VP process, details of the latter are summarized in Table III: (1) the vibrational energy gap associated to the $\Delta v' = -1$ channel, $\Delta\mathcal{E}_{\text{Br}_2}^{B, v'-1} = \mathcal{E}_{\text{Br}_2}^{B, v'} - \mathcal{E}_{\text{Br}_2}^{B, v'-1}$; (2, 3) NeBr_2^{14} and Ne_2Br_2 binding energies, $D_0^{\text{NeBr}_2(B, v')} = -\mathcal{E}_{\text{NeBr}_2}^{B, v'}$ and $D_0^{B, v'} = -\mathcal{E}^{B, v'}$; and (4, 5) the energies available after dissociation of the first and second Ne atoms via, respectively, the $\Delta v' = -1, -2$ channels, *i.e.* $E_{\text{avail}}^{v'-1}$ and $E_{\text{avail}}^{v'-2}$.

Tests on basis-set convergence yield an estimate for the accuracy of our $D_0^{B, v'}$ values of about 1 cm^{-1} (any further improvement was considered unnecessary for our purposes here). These theoretical values are just slightly different from the 141 cm^{-1} estimate of Pio *et al.*⁴⁷, and suggest an interaction energy for the Ne–Ne bond of about $10\text{--}12 \text{ cm}^{-1}$, which is to be compared with the 17 cm^{-1} of isolated Ne_2 used in Ref. 47. Our predictions are, however, consistent with the value of 12.81 cm^{-1} in Ref. 11 for the effective Ne–Ne bond. Moreover, our calculations predict an average Ne–Ne interatomic distance at the minimum energy structure of about 3.2 \AA (within 3.8% of the value for Ne_2 , see Table I), also in good agreement with the estimate in Ref. 11. It is important to note that all values in Table III, except for $D_0^{\text{NeBr}_2(B, v')}$, are theoretical predictions based on the B -state PES used in this work. This is the reason for small discrepancies with some experimental predictions⁴⁷. For instance, we estimate the closing of the $\Delta v' = -1$ channel for the dissociation of the first Ne atom to occur at $v' = 25$, as opposed to the experimental $v' = 23$. Also, complete dissociation via the $\Delta v' = -2$ channel would be energetically accessible up to $v' = 27$ (instead of $v' = 25$).

1. Vibrational branching ratios

Experimental and QCT vibrational branching ratios after the dissociation of one Ne atom, $\text{NeBr}_2(v' - n):\text{NeBr}_2(v' - 1)$, and two Ne atoms, $\text{Br}_2(v' - n):\text{Br}_2(v' - 2)$, are given in Table IV. It is readily apparent that QCT fails to capture the physics behind the vibrational distributions in the VP process, irrespectively of the statistical procedure (SB or GW) employed. This is a general effect of the large mismatch in the strengths of the different DOF involved in the VP of vdW clusters, at least for moderate vibrational excitations of the chemically-bounded diatom. The same behavior may therefore be expected in similar systems. In the absence of resonances, such a mismatch causes the energy transfer from the vibrational to the vdW dissociation modes to be very inefficient. This is remarkably different from the unimolecular dissociation of more conventional, *i.e.* chemically-bounded, molecules, where statistical arguments are usually applicable at least for the DOF directly involved in the fragmentation. In the classical description of the VP of Ne_2Br_2 , the Br_2 vibrational energy gradually ‘flows’ into the vdW modes and eventually becomes large enough for dissociation to occur. A very limited number of the accessible final vibrational states is hence populated, the distributions being highly non-statistical (Fig. 3). In addition, due to the very low density of vibrational states, the classical picture dramatically differs from the quantum-mechanical description and hence the experimental observations. This is particularly clear from SB product branching ratios. In this case, the loss of 1.5 ‘quanta’ provides enough energy to eject both Ne atoms up to $v' = 22$ (Table III), which is reflected in nonphysical trajectories dissociating via the $\Delta v' = -1$ channel (Table IV). The main advantage of GW over SB results in this case is to populate the qualitatively correct vibrational channels. However, as discussed above, the classical description is intrinsically inadequate and GW predicts a larger than observed propensity for $\Delta v' = -1$ and -2 channels for the respective dissociation of the first and second Ne atoms. Also, the increasing importance of highly state-specific IVR (sparse regime) predicted in the experiment for states above $v' = 19$ cannot be adequately reproduced within QCT. Some additional discrepancies, *e.g.* in channels closings, are due to the PES employed and have been already discussed at the end of Sec. III C.

2. Rotational distributions

Together with vibrational distributions, product rotational state distributions provide a more detailed picture of the VP process than dissociation lifetimes. In particular, they contain important information on the anisotropy of the PES, the vibrational level spacings and the effects of IVR and resonances on the fragmentation dynamics⁵⁸. Rotational distributions corresponding to various initial v' levels for the NeBr_2 intermediate tri-

TABLE IV. Experimental⁴⁷ and theoretical (this work) branching ratios in the vibrational predissociation of Ne₂Br₂(*B*, *v*').

<i>v</i> '	NeBr ₂ (<i>v</i> ' - <i>n</i>):NeBr ₂ (<i>v</i> ' - 1)			Br ₂ (<i>v</i> ' - <i>n</i>):Br ₂ (<i>v</i> ' - 2)			
	(<i>v</i> ' - 2)	(<i>v</i> ' - 3)	(<i>v</i> ' - 4)	(<i>v</i> ' - 1)	(<i>v</i> ' - 3)	(<i>v</i> ' - 4)	(<i>v</i> ' - 5)
16 Experiment				0.16			
QCT: SB/GW	0.04/0.27			0.98/0.0			
17 Experiment				0.31	0.05		
QCT: SB/GW	0.08/0.29			0.48/0.0			
18 Experiment				0.33	0.08		
QCT: SB/GW	0.16/0.35			0.20/0.0	0.01/0.0		
19 Experiment				0.45	0.09		
QCT: SB/GW	0.28/0.45			0.07/0.0	0.02/0.01		
20 Experiment				0.65	0.13	0.03	
QCT: SB/GW	0.47/0.56	0.01/0.01		0.02/0.0	0.05/0.03		
21 Experiment				0.97	0.29		
QCT: SB/GW	0.71/0.73	0.02/0.02		0.01/0.0	0.10/0.06		
22 Experiment				1.58	0.51	0.17	
QCT: SB/GW	1.04/0.92	0.06/0.04		0.01/0.0	0.18/0.10	0.01/0.0	
23 Experiment				3.28	1.37	0.49	
QCT: SB/GW	1.52/1.22	0.15/0.09	0.01/0.0	0.29/0.15	0.02/0.01		

atomic complex and the Br₂ diatomic product are depicted in panels a and b of Fig. 5 respectively. Only the GW results are shown because even if just a few vibrational states are populated, the SB and GW curves are only slightly different. This is not particularly surprising; although the available energy more than halves in the range of *v*' considered (Table III), the tail of QCT distributions rapidly tend to zero before this effect becomes important.

The rotational state of the NeBr₂ intermediate complex was calculated from $\mathbf{j} + \mathbf{l}_{1(2)} = -\mathbf{l}_{2(1)}$, which is valid only for $\mathbf{J} = \mathbf{0}$. As seen in panel (a), the dissociation of the first Ne atom leaves the resultant triatomic complex in a highly-excited rotational state. The corresponding distribution extends over more than 30 rotational levels and peaks around 8–10. Such rotational excitation, together with the additional excitation of the vdW vibrations, are expected to be the cause for the lifetime of the intermediate molecule being larger than that of the directly excited triatomic complex. This effect has been observed in the experiment⁴⁷ and is reproduced by our QCT calculations, as seen by comparing the corresponding lifetimes in Table II with the QCT predictions in Table 1 of Ref. 31.

The GW rotational distributions for the Br₂ product, shown in panel (b), extend over the full range of accessible states determined by the maximum available energy in Table III. For the sake of comparison, the initial distribution $P^X(j)$ has also been included in this panel. In the particular case of $\mathbf{J} = \mathbf{0}$, symmetry considerations for the ground state are only responsible for even *j* values contributing in $P^X(j)$ ⁶². In general, the calculated rotational distributions are considerably hotter for the

products, with a maximum at about $j^f = 6-8$ almost independent of *v*', than for the initial states. The initial and final distributions have, nevertheless, similar shapes. Although experimental rotational distributions were not reported in the experiment⁴⁷, a few points can be made with respect to QCT predictions: (a) the Boltzmann-like shape seems to be consistent with experimental measurements for the directly excited NeBr₂ molecule¹⁴, and previous QCT calculations^{31,35}; and (b) the Br₂ product is more rotationally excited than in the photo-dissociation of NeBr₂^{14,31,35}, for which the distributions peak about $j^f = 4-6$. The extent of the QCT distributions may be expected to differ from future experimental measurements due to the PES employed (see discussion at the end of Sec. III C), particularly close to a channel closing.

IV. SUMMARY AND CONCLUSIONS

We have studied the vibrational predissociation (VP) of the Ne₂Br₂(*B*, *v*' = 16–23) van der Waals (vdW) cluster using the quasi-classical trajectory (QCT) and the (Cartesian) coupled coherent states (CCS) methods.

A sequential mechanism was used to fit the dynamical evolution of the different complexes involved. Both QCT and CCS are shown to provide very good estimates for the different dissociation lifetimes reported in the experiment⁴⁷ and previous molecular dynamics with quantum transitions (MDQT) simulations¹¹. QCT predictions are, however, obtained at a much lower computational expense. Various sources of non-exponential behavior have been identified and their implications extensively discussed. In particular, the initial shape of

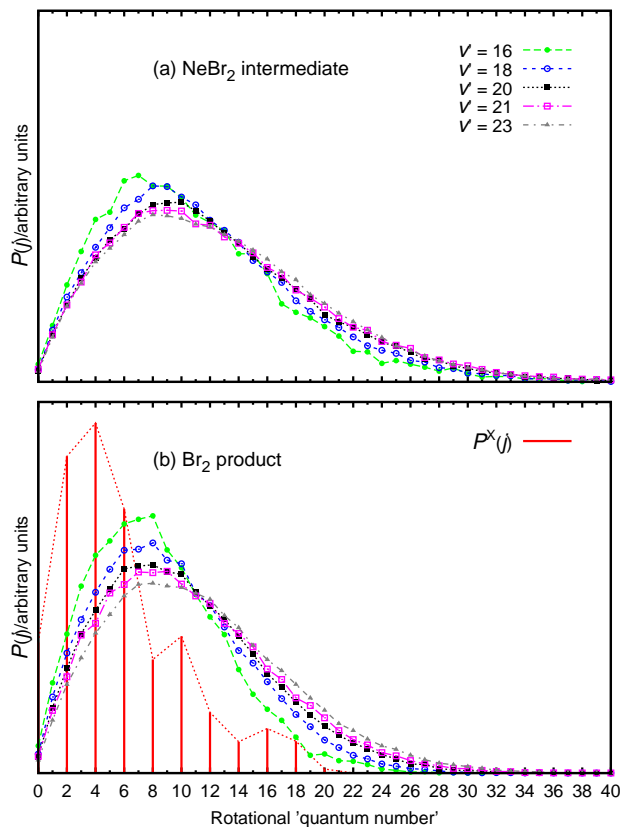


FIG. 5. (Color online) Rotational distributions in the vibrational predissociation of $\text{Ne}_2\text{Br}_2(B)$, for: (a) NeBr_2 intermediate complex; and (b) Br_2 diatomic product. $P^X(j)$ is the quantum distribution used to generate the quasi-classical initial conditions.

the QCT curves at short times arises from the ‘non-democratic’ selection of classical initial conditions and the classical description of the process. Meanwhile, the quantum CCS simulations give curves whose initial shape is in much better agreement with the experimental observations⁴⁷. However, the basis functions used to describe the wave function follow dissociative trajectories. The high dimensionality of the phase space therefore results in the basis functions decoupling and thus a semi-classical description of the cluster. This change is at least partially responsible for the departure at longer times of the curves from their initial exponential shape. An intrinsic multi-step dissociation mechanism, as observed in the experiment⁴⁷ and predicted by MDQT calculations¹¹, may also be responsible for such non-exponential behavior at long times. Additional calculations are needed in order to clarify this issue. The time scale over which the CCS gives a good description was increased significantly to around 15 ps by re-expanding the dissociated basis functions. Despite this improvement, the QCT simulations give curves that agree much more closely with the experimental results at longer times. The behavior of the QCT curves at longer times is, however, affected by

low-dimensional tori in classical phase space. These tori are mainly in the form of quasi-periodic trajectories and are partially due to the weakness of vdW interactions. In both QCT and CCS calculations, the percentage of trajectories which correspond to the concerted mechanism is practically negligible, below 0.1% for QCT and about 2% for CCS. In this regard, it is important to note that trajectory-based approaches like CCS may become more effective than ‘standard’ quantum methods, mainly because they allow analyzing the different mechanisms by simply inspecting the trajectories.

As in our previous work with QCT on triatomic vdW molecules³⁵, we found that application of the Gaussian weighting (GW) procedure yields survival probability curves, and consequently lifetimes, which are not significantly different from those calculated using the standard binning (SB) procedure. In addition, the capabilities of QCT in the description of the fragmentation kinetics was analyzed in detail by using reduced-dimensionality models of the complexes and concepts from phase-space transport theory.

We have reported QCT ro-vibrational product state distributions for the intermediate and final states of the VP process, and compared the vibrational distributions with the experimental results of Pio *et al.*⁴⁷. As in previous studies, *e.g.* Ref. 35, the SB was found to populate nonphysical dissociation channels ($\Delta v' = -1$ in this case). This is due to energetic issues and can be easily solved by using the GW method. The latter, however, predicts a larger than observed propensity for dissociation of the first (second) Ne atom via the $\Delta v' = -1$ (-2) channel. We argued that this is a general problem in the classical description of the VP of vdW clusters, which may be attributed to the weakness of vdW interactions. Due to the latter, the characteristic frequencies for the diatomic subunit are usually one or more orders of magnitude larger than those of the bending mode within the vdW well. The energy transfer leading to dissociation is inefficient and slow. To complicate matters further, as energy flows from the vibrational to the transitional modes, the vdW bending modes evolve from bounded, through hindered, to free type of motion and the role of many non-linear resonances become increasingly important⁴². This fact additionally worsens the quality of any classical description of the VP process, since quantum state-selectivity cannot be adequately described. As expected, the quantum-classical discrepancies will be more pronounced for relatively low v' , given the very low density of vibrational states.

Dissociation of the first Ne atom leaves the NeBr_2 in a highly-excited rotational state. This rotational excitation, and the additional excitation of the vdW vibration, are responsible for an increase dissociation lifetime of the intermediate complex, as compared to the lifetime of the directly excited NeBr_2 . This effect was observed in the experiment⁴⁷ and is correctly predicted by our calculations. Product Br_2 rotational distributions are found to be significantly hotter in the products, extending over

the full range of available energies.

ACKNOWLEDGMENTS

WAG, MLGM and JRS wish to thank Prof. Gerardo Delgado-Barrio, from the Consejo Superior de Investigaciones Científicas, España, for his contribution in the calculation of quasi-classical initial distributions. These authors wish also to acknowledge the support from the PNCB/2/9 project of the Departamento de Física General in the Instituto Superior de Tecnologías y Ciencias Aplicadas, Cuba. SKR would like to thank the EPSRC for funding through grant number EP/E009824/1 and more recently the University of Leeds for a Visiting Research Fellowship. SKR would also like to acknowledge the use of the UK National Grid Service (NGS) and the University of Leeds central HPC system in performing the CCCS simulations. The collaboration between the Cuban and British groups was possible thanks to an International Joint Project grant from the Royal Society.

- ¹W. Sharfin, K. E. Johnson, L. Wharton, and D. H. Levy, *J. Chem. Phys.* **71**, 1292 (1979).
- ²J. E. Kenny, K. E. Johnson, W. Sharfin, and D. H. Levy, *J. Chem. Phys.* **72**, 1109 (1980).
- ³B. A. Swartz, D. E. Brinza, C. M. Western, and K. C. Janda, *J. Phys. Chem.* **88**, 6272 (1984).
- ⁴R. E. Smalley, D. H. Levy, and L. Wharton, *J. Chem. Phys.* **64**, 3266 (1976).
- ⁵G. Kubiak, P. S. H. Fitch, L. Wharton, and D. H. Levy, *J. Chem. Phys.* **68**, 4477 (1978).
- ⁶K. E. Johnson, W. Sharfin, and D. H. Levy, *J. Chem. Phys.* **74**, 163 (1981).
- ⁷J. A. Beswick and J. Jortner, *J. Chem. Phys.* **69**, 512 (1979).
- ⁸J. A. Beswick, J. Jortner, and G. Delgado-Barrio, *J. Chem. Phys.* **70**, 3895 (1979).
- ⁹M. A. Taylor, J. M. Pio, W. E. van der Veer, and K. C. Janda, *J. Chem. Phys.* **132**, 104309 (2010).
- ¹⁰B. Miguel, A. Bastida, J. Zúñiga, A. Requena, and N. Halberstadt, *J. Chem. Phys.* **113**, 10130 (2000).
- ¹¹B. Miguel, A. Bastida, J. Zúñiga, A. Requena, and N. Halberstadt, *Faraday Discuss.* **118**, 257 (2001).
- ¹²D. D. Evard, C. R. Bieler, J. I. Cline, N. Sivakumar, and K. C. Janda, *J. Chem. Phys.* **89**, 2829 (1988).
- ¹³A. Rohrbacher, T. Ruchti, K. C. Janda, A. A. Buchachenko, M. I. Hernández, T. González-Lezana, P. Villarreal, and G. Delgado-Barrio, *J. Chem. Phys.* **110**, 256 (1999).
- ¹⁴M. Nejad-Sattari and T. A. Stephenson, *J. Chem. Phys.* **106**, 5454 (1997).
- ¹⁵A. Rohrbacher, N. Halberstadt, and K. C. Janda, *Annu. Rev. Phys. Chem.* **51**, 405 (2000).
- ¹⁶T. González-Lezana, M. I. Hernández, G. Delgado-Barrio, A. A. Buchachenko, and P. Villarreal, *J. Chem. Phys.* **105**, 7454 (1996).
- ¹⁷T. González-Lezana, M. I. Hernández, G. Delgado-Barrio, and P. Villarreal, *J. Chem. Phys.* **106**, 3216 (1997).
- ¹⁸T. A. Stephenson and N. Halberstadt, *J. Chem. Phys.* **112**, 2265 (2000).
- ¹⁹O. Roncero, J. Campos-Martínez, M. I. Hernández, G. Delgado-Barrio, P. Villarreal, and J. Rubayo-Soneira, *J. Chem. Phys.* **115**, 2566 (2001).
- ²⁰A. García-Vela and K. C. Janda, *J. Chem. Phys.* **124**, 034305 (2006).
- ²¹A. García-Vela, *J. Chem. Phys.* **126**, 124306 (2007).
- ²²A. García-Vela, *J. Chem. Phys.* **129**, 094307 (2008).
- ²³C. Meier and U. Manthe, *J. Chem. Phys.* **115**, 5477 (2001).
- ²⁴A. García-Vela, *J. Chem. Phys.* **122**, 014312 (2005).
- ²⁵A. Bastida, J. Zúñiga, A. Requena, N. Halberstadt, and J. A. Beswick, *J. Chem. Phys.* **109**, 6320 (1998).
- ²⁶S. Fernández-Alberti, N. Halberstadt, J. A. Beswick, A. Bastida, J. Zúñiga, and A. Requena, *J. Chem. Phys.* **111**, 239 (1999).
- ²⁷A. Bastida, B. Miguel, J. Zúñiga, A. Requena, N. Halberstadt, and K. C. Janda, *J. Chem. Phys.* **111**, 4577 (1999).
- ²⁸J. Rubayo-Soneira, A. García-Vela, G. Delgado-Barrio, and P. Villarreal, *Chem. Phys. Lett.* **243**, 236 (1995).
- ²⁹A. García-Vela, J. Rubayo-Soneira, G. Delgado-Barrio, and P. Villarreal, *J. Chem. Phys.* **104**, 8405 (1996).
- ³⁰R. L. Waterland, J. M. Skene, and M. I. Lester, *J. Chem. Phys.* **89**, 7277 (1988).
- ³¹M. L. González-Martínez, J. Rubayo-Soneira, and K. C. Janda, *Phys. Chem. Chem. Phys.* **8**, 4550 (2006).
- ³²R. L. Waterland, M. I. Lester, and N. Halberstadt, *J. Chem. Phys.* **92**, 4261 (1990).
- ³³L. Bonnet and J.-C. Rayez, *Chem. Phys. Lett.* **277**, 183 (1997).
- ³⁴L. Bonnet and J.-C. Rayez, *Chem. Phys. Lett.* **397**, 106 (2004).
- ³⁵M. L. González-Martínez, W. Arbelo-González, J. Rubayo-Soneira, L. Bonnet, and J.-C. Rayez, *Chem. Phys. Lett.* **463**, 65 (2008).
- ³⁶J. I. Cline, N. Sivakumar, D. D. Evard, C. R. Bieler, B. P. Reid, N. Halberstadt, S. R. Hair, and K. C. Janda, *J. Chem. Phys.* **90**, 2605 (1989).
- ³⁷M. J. Davis and S. K. Gray, *J. Chem. Phys.* **84**, 5389 (1986).
- ³⁸S. K. Gray, *J. Chem. Phys.* **87**, 2051 (1987).
- ³⁹R. E. Gillilan and G. S. Ezra, *J. Chem. Phys.* **94**, 2648 (1991).
- ⁴⁰M. Zhao and S. A. Rice, *J. Chem. Phys.* **96**, 3542 (1992).
- ⁴¹M. Zhao and S. A. Rice, *J. Chem. Phys.* **96**, 6654 (1992).
- ⁴²A. A. Granovsky, A. V. Medvedev, A. A. Buchachenko, and N. F. Stepanov, *J. Chem. Phys.* **108**, 6282 (1998).
- ⁴³R. Prosimiti, P. Villarreal, G. Delgado-Barrio, and O. Roncero, *Chem. Phys. Lett.* **359**, 229 (2002).
- ⁴⁴R. Sospedra-Alfonso, L. Velázquez, and J. Rubayo-Soneira, *Chem. Phys. Lett.* **375**, 261 (2003).
- ⁴⁵M. L. González-Martínez and J. Rubayo-Soneira, *Rev. Cub. Física* **22**, 48 (2005), in Spanish.
- ⁴⁶M. Gutmann, D. M. Willberg, and A. H. Zewail, *J. Chem. Phys.* **97**, 8048 (1992).
- ⁴⁷J. M. Pio, M. A. Taylor, W. E. van der Veer, C. R. Bieler, J. A. Cabrera, and K. C. Janda, *J. Chem. Phys.* **133**, 014305 (2010).
- ⁴⁸S. K. Reed, D. R. Glowacki, and D. V. Shalashilin, *Chem. Phys.* **370**, 223 (2010).
- ⁴⁹S. K. Reed, M. L. González-Martínez, J. Rubayo-Soneira, and D. V. Shalashilin, *J. Chem. Phys.* **134**, 054110 (2011).
- ⁵⁰A. Valdés, R. Prosimiti, P. Villarreal, and G. Delgado-Barrio, *J. Chem. Phys.* **122**, 044305 (2005).
- ⁵¹A. Valdés, R. Prosimiti, P. Villarreal, and G. Delgado-Barrio, *J. Chem. Phys.* **125**, 014313 (2006).
- ⁵²R. F. Barrow, T. C. Clark, J. A. Coxon, and K. K. Lee, *J. Mol. Spectrosc.* **51**, 428 (1974).
- ⁵³A. A. Buchachenko, A. Y. Baisogolov, and N. F. Stepanov, *J. Chem. Soc., Faraday Trans.* **90**, 3229 (1994).
- ⁵⁴F. Y. Naumkin and P. J. Knowles, *J. Chem. Phys.* **103**, 3392 (1995).
- ⁵⁵A. Rohrbacher, J. Williams, and K. C. Janda, *Phys. Chem. Chem. Phys.* **1**, 5263 (1999).
- ⁵⁶R. Prosimiti, C. Cunha, A. A. Buchachenko, G. Delgado-Barrio, and P. Villarreal, *J. Chem. Phys.* **117**, 10019 (2002).
- ⁵⁷J. M. Pio, W. E. van der Veer, C. R. Bieler, and K. C. Janda, *J. Chem. Phys.* **128**, 134311 (2008).
- ⁵⁸R. Schinke, *Photodissociation Dynamics* (Cambridge University Press, Cambridge, 1993).
- ⁵⁹J. Rubayo-Soneira, *Estudio de la predissociación de sistemas triatómicos y tetraatómicos de van der Waals*, Ph.D. thesis, Consejo Superior de Investigaciones Científicas, Madrid, España (1995), in Spanish.
- ⁶⁰A. J. Lichtenberg and M. A. Lieberman, *Regular and Stochastic*

- Motion* (Springer-Verlag, New York, 1993).
- ⁶¹After assuming that strong IVR makes all available configurations equally populated within an induction time relatively short compared to the time scale of the process of interest, classical initial conditions are computed using microcanonical distributions.
- ⁶²P. Villarreal, O. Roncero, and G. Delgado-Barrio, *J. Chem. Phys.* **101**, 2217 (1994).
- ⁶³G. Delgado-Barrio, A. García-Vela, C. García-Rizo, M. I. Hernández, and P. Villarreal, *Mol. Eng.* **7**, 219 (1997).
- ⁶⁴W. H. Miller, *Adv. Chem. Phys.* **25**, 69 (1974).
- ⁶⁵R. N. Porter and L. M. Raff, in *Dynamics of Molecular Collisions, Part B*, edited by W. H. Miller (Plenum Press, New York, 1976).
- ⁶⁶G. Czako and J. M. Bowman, *J. Chem. Phys.* **131**, 244302 (2009).
- ⁶⁷L. Bonnet and J. Espinosa-García, *J. Chem. Phys.* **133**, 164108 (2010).
- ⁶⁸W. H. Press, S. A. Teukolsky, W. T. Vetterling, and B. T. Flannery, *Numerical recipes. The art of scientific computing.*, 3rd ed. (Cambridge University Press, Cambridge, 2007).
- ⁶⁹S. K. Reed, M. L. González-Martínez, W. Arbelo-González, J. Rubayo-Soneira, and D. V. Shalashilin, (2012), in preparation.
- ⁷⁰M. J. Davis, *J. Chem. Phys.* **83**, 1016 (1985).
- ⁷¹S. K. Gray, S. A. Rice, and M. J. Davis, *J. Phys. Chem.* **90**, 3470 (1986).
- ⁷²M. Zhao and S. A. Rice, *J. Chem. Phys.* **96**, 7483 (1992).
- ⁷³In order to further distinguish between C_1 and C_2 events in Scheme 1, the Ne-Ne energy was checked for compatibility with formation of a Ne₂ molecule.
- ⁷⁴One may consider the case where the initial dissociation step leads—for a significant part of the ensemble—to states ‘trapped’ behind large centrifugal barriers, *i.e.* orbiting resonances. These would act as effective bottlenecks to the dissociation of the triatomic intermediate complex and result in a slightly more complicated kinetic mechanism, as in Ref. 29. In such cases, the rotational angular momentum of the intermediate complex would result statistically correlated with $t_2^i - t_1^i$.
- ⁷⁵J. A. Cabrera, C. R. Bieler, B. C. Ölbricht, W. E. van der Veer, and K. C. Janda, *J. Chem. Phys.* **123**, 054311 (2005).
- ⁷⁶D. L. Bunker and W. L. Hase, *J. Chem. Phys.* **59**, 4621 (1973).
- ⁷⁷R. Paškauskas, C. Chandre, and T. Uzer, *Phys. Rev. Lett.* **100**, 083001 (2008).